Silica–ZnO Nanotubes

DOI: 10.1002/ange.200803203

Bubble-Templated and Flow-Controlled Synthesis of Macroscopic Silica Tubes Supporting Zinc Oxide Nanostructures**

*Jason J. Pagano, Tamás Bánsági, Jr., and Oliver Steinbock**

Reaction–transport coupling can self-organize inorganic structures with complex, hierarchical architectures that in some cases extend beyond the nanometer scale into the macroscopic world. A simple but nonetheless interesting example is the hollow-tube motif which is found in cement,[1] biomineralized shells of algae,[2] ferrotubes,[3] speleotherms[4] and hydrothermal vents.[5] Arguably one of the best laboratory models for the study of tube formation is a class of reactions known as chemical or silica "gardens". These reactions produce millimeter-scale precipitation tubes that can grow upward at rates of millimeters per second.[6] Recent studies of these hollow structures have demonstrated applications of metallosilica tubes as Brønsted acid catalysts[7] and simple microfluid devices.[8] Herein, we present the synthesis of similar tubes using a flow injection method[9] with gas bubbles as directional guides and templates. The bubbles are pinned to the interfacial reaction zone of the growing tubes. The resulting materials are very straight tubes consisting of silica-supported zinc oxide nanostructures and show interesting luminescence and photocatalytic properties.

The prototypical experiment underlying our investigations consists of crystals seeded into aqueous solutions containing anions such as borates, phosphates,[10] carbonates,[11] or silicates; herein we present experiments involving silicates. Furthermore, many different salts can be used as the seed, with the exception of Group 1 elements. Tube morphogenesis starts with the formation of a colloidal and semipermeable membrane around the dissolving seed. Osmotic pressure differences induce a cross-membrane flux of water and subsequently rupture the membrane. From the breach site a buoyant jet of salt solution is ejected which templates the tube-forming co-precipitation of amorphous silica and metal hydroxides (or oxides).

Figure 1a shows a precipitation structure formed from a zinc(II) sulfate crystal seeded into 2.5 M silicate solution. The tube is reminiscent of an erratic string of beads. Figure 1b shows a micrograph of a similar tube obtained by scanning electron microscopy (SEM). The average diameter of the tube is about 1 mm. Clearly, such irregular and uncontrolled structures have very limited value as hollow support systems and cannot be extended over long distances. Our method overcomes these limitations by replacing the seed particle with a seed solution injected at constant flow rates. Furthermore, we place a buoyant gas bubble into the initial, colloidal

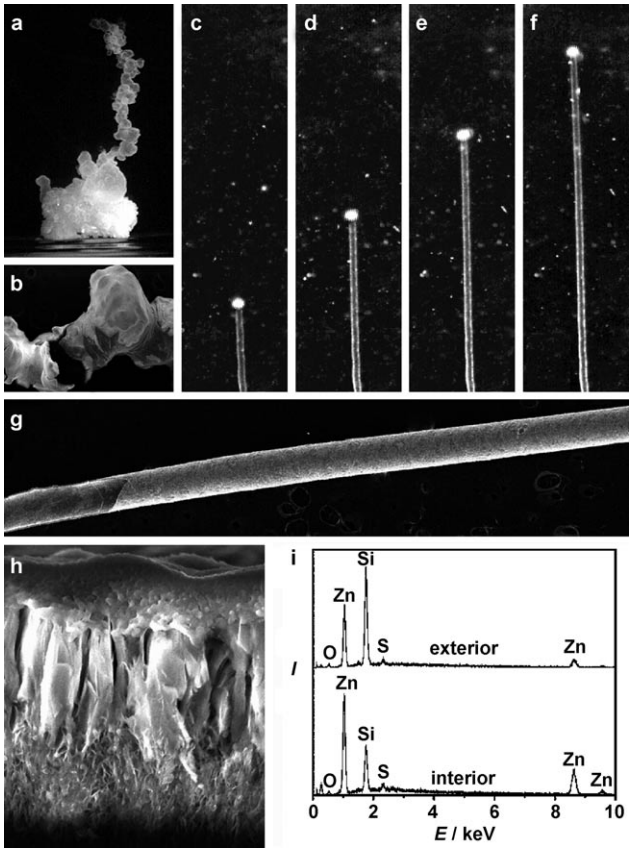

Figure 1. a) Structure formed from a $ZnSO_4$ crystal seeded into a silicate solution. Field of view corresponds to 4.7×7.1 cm^2. b) SEM of a similar tube. Image area corresponds to 2.5×1.9 mm^2. c–f) The sequence of images as a gas bubble guides the injection-controlled growth of a precipitation tube. Time between frames: 300 ms; image height corresponds to 1 cm. g) SEM of a bubble-guided heat-treated zinc-silica tube. Image area corresponds to 7.5×1.7 mm^2. h) SEM of the tube wall showing the exterior surface in the upper region. Image area corresponds to 11×13 μm^2. i) EDS spectra of the exterior and interior of the tube surface.

[*] Dr. T. Bánsági, Jr., Prof. O. Steinbock
Florida State University
Department of Chemistry and Biochemistry
Tallahassee, FL 32306-4390 (USA)
Fax: (+1) 850-644-8281
E-mail: steinbck@chem.fsu.edu
Prof. J. J. Pagano
Saginaw Valley State University
Department of Chemistry
University Center, MI 48710 (USA)

[**] This work was supported by the American Chemical Society Petroleum Research Fund (Grant No. 42798-AC10) and the National Science Foundation (Grant No. 0513912). We thank Dr. Eric Lochner and Dr. Yan Xin for assistance.

Supporting information for this article is available on the WWW under http://dx.doi.org/10.1002/anie.200803203.

membrane that is formed at the injection nozzle. These simple but radical modifications of the prototypical experiment allow us to produce extremely linear tubes of uniform diameter in a controlled fashion. The reproducibility is very high, but requires careful placement of the bubble-delivering needle.

This result is illustrated by the image sequence in Figure 1 c–f. It shows an initially translucent, later white precipitation tube growing upwards in a 1.0 M sodium silicate solution (dark background). On average, the tube is 0.66 mm wide and confines the steadily injected zinc(II) sulfate solution within its expanding structure. As a small air bubble (white spot) is pinned to the top of the tube, the tube starts growing vertically from the bubble/tube interface, and not along or at the base of the tube. The pinned bubble moves upward at a constant speed of 0.7 $cm\,s^{-1}$, which is much smaller than the velocity of a free rising bubble. The observed velocity v is in good agreement with the simple equation $v = Q/\pi r^2$ that expresses perfect volume conservation of the injected solution in the growing tube in terms of the pump rate Q and the tube radius r. In this example, Q and r are 10.0 $mL\,h^{-1}$ and 0.33 mm, respectively, yielding $Q/\pi r^2 = 0.8\ cm\,s^{-1}$.

The resulting tubes can be easily collected, washed, and dried for further characterization and physicochemical modification. The SEM image in Figure 1 g shows a tube synthesized using our bubble-guided injection technique. The tube as shown is very straight and its radius remarkably uniform (here 240 μm), which is about 70–80 % of the bubble radius. By varying the size of the injected bubbles, we have generated tubes with radii from 180 to 450 μm.

To demonstrate possible post-synthesis modifications of the tubes, we explore heat-induced structural and chemical changes. The specific goal is to convert zinc hydroxide within the tube wall into technologically more relevant zinc oxide. Tubes are pre-dried at room temperature and then heated to approximately 250 °C under ambient conditions. Visual inspection of the resulting samples shows that nearly all tubes are intact. Furthermore, their length, radius, color, and surface texture remain qualitatively unchanged. However, thermogravimetric analyses show maximum weight loss around 70 °C (data given in Supporting Information). As crystalline $Zn(OH)_2$ is known to yield ZnO in the temperature range of 70 to 140 °C,[12] the loss of weight suggests the formation of ZnO within the tube wall.

Figure 1 h shows a SEM image of the wall of a heat-treated tube. The wall is approximately 10 μm thick, which appears to be characteristic for our method within the investigated range of experimental parameters. The outer and inner tube surfaces extend along the upper and lower side of the image, respectively and show marked differences. The exterior half of the wall has a glassy appearance and consists of columnar structures that are oriented normal to the surface. The interior half is more intricate and reminiscent of a random network of fibers.

Figure 1 i shows typical results of energy dispersive X-ray spectroscopy (EDS) as performed for the exterior (top trace) and interior (bottom trace) surface of a heat-treated tube. As expected, these SEM-EDS data characterize both wall surfaces as rich in silicon and zinc. Furthermore, the detected zinc-to-silicon mass ratio is 1.39 and 0.43 for the inner surface and the outer surface, respectively. The corresponding mole ratios $n_{Zn}/(n_{Zn}+n_{Si})$ are 0.37 and 0.16, respectively, suggesting an amorphous silica matrix with a zinc-rich interior.

We note that the observed composition gradient does not occur during heating but is caused by the specific compartmentalization of zinc, silicate, and hydroxide ions during the initial formation of the tube. Specifically, it stems from the reaction conditions within the topmost growth region where the outer silicate solution is separated from a small volume of zinc solution. It is likely that the two distinct morphologies across the tube wall observed by SEM (cf. Figure 1 h) correlate with regions of high and low zinc content.

To obtain further information on the microscopic morphology and chemical structure of the tube wall, we recorded high-resolution SEM pictures of tubes having exposed zinc-rich interior surfaces. A typical example is shown Figure 2 a and b and has a flake- or needle-like morphology. The length of the individual nanostructures varies between 1 μm and 4 μm, whereas their thickness is below 100 nm. We note that ZnO nanotubes and rods of similar dimensions have been grown using chemical vapor deposition.[13]

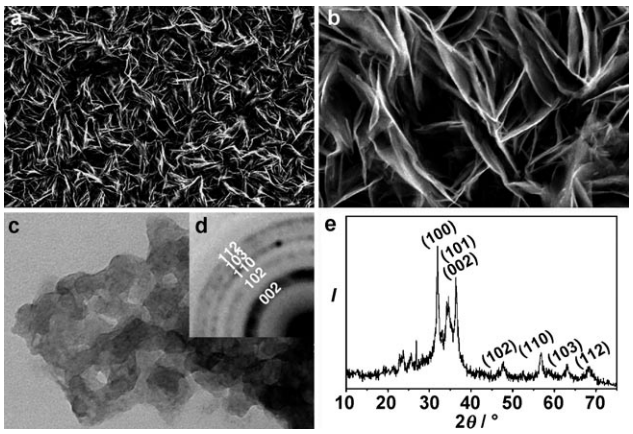

Figure 2. Bubble-guided tubes after heating to 250 °C. a,b) SEM images of the interior surface of the heated tubes. Image areas: a) 51 × 33 μm^2, b) 11 × 7 μm^2. c) HRTEM image of tube fragments. Image area: 215 × 150 nm^2. d) SAED ring patterns and corresponding Miller indices. e) X-ray diffraction pattern of tube fragments.

High-resolution transmission electron microscopy (HRTEM) provides additional insights into the chemical nature of the nanostructured tubes. The representative HRTEM image in Figure 2 c shows particles with a mean diameter in the range of 10–30 nm. A corresponding selected area electron diffraction (SAED) pattern (Figure 2 d) shows five intense rings. These rings correspond to the Miller indices (112), (103), (110), (102), and (002), which are characteristic of zinc(II) oxide.

The powder X-ray diffraction (XRD) pattern in Figure 2 e complements the SAED pattern. The X-ray data show that the tube contains sufficient amounts of crystalline material to allow for a reliable assignment. We find seven characteristic peaks ($2\theta = 31.9$, 34.2, 36.2, 47.7, 56.7, 63.1, 68.1°), each

labeled by the respective Miller index of ZnO, indicating that the observed structures are composed of hexagonal zinc oxide nanoparticles with a zincite structure (Powder Diffraction File 36-1451). Note that we did not observe a broad pattern around $2\theta = 20°$, which would be expected for crystalline SiO_2. There is also no evidence for the presence of zinc silicates.

To estimate the mean crystalline size s from the XRD pattern, we use the Scherrer equation $s = K\lambda/\Delta(2\theta)\cos(\theta)$, where λ is the X-ray wavelength (for $Cu_{K\alpha}$, that is, $\lambda = 0.154$ nm), $\Delta(2\theta)$ is the peak width at half maximum, and $K = 0.9$.[14] This analysis yields sizes in the range of $s = 7$–23 nm for the seven major peaks. Overall these values are in agreement with the particle dimensions measured by image analysis of our HRTEM data.

The heat-treated precipitation tubes also have interesting optical features, as exemplified by their photoluminescence (Figure 3a). When excited with ultraviolet light at $\lambda = 325$ nm, the silica/ZnO tubes emit band-edge luminescence near 415 nm (2.99 eV), accompanied by a broad green emission around 522 nm (2.38 eV). A similar but much narrower emission band (centered at 395 nm) has been reported for non-tubular composites with highly dispersed ZnO within silica pores.[15] The green emission in our experiments may result from oxygen vacancies[16] in the tube wall.

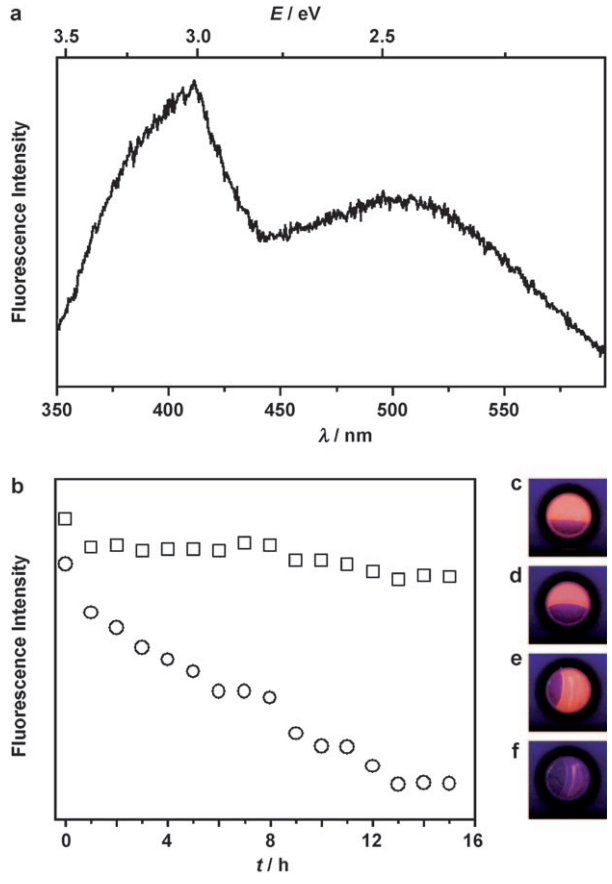

Figure 3. a) Photoluminescence spectrum of silica/ZnO tubes excited at 325 nm. b) Fluorescence intensity as a function of time for the photodegradation of rhodamine B catalyzed by short tube segments (open circles) and for tube-free control samples (open squares). Corresponding fluorescence micrographs of c) the initial control sample, d) the control after 15 h, e) the initial, catalyzed sample, and f) the latter after 15 h. Diameter of disk-shaped container: 1 cm.

The photocatalytic activity of the silica-supported ZnO tubes is analyzed by qualitative measurements of the photodegradation of the dye rhodamine B (RhB). For these fluorescence measurements, small disk-shaped containers were filled with 5 μM aqueous solution of RhB and were divided into two groups. One group of these containers contained single, heat-activated zinc oxide/silica tubes, whereas the others served as controls. The containers were covered with quartz lids and sealed to avoid evaporation. They were then exposed to UV light, and their fluorescence signals are measured as functions of time. Figure 3b shows two typical signal traces obtained by spatial averaging over a "tube-free" control (open squares) and a sample containing three, approximately 5 mm-long segments of silica/ZnO tubes (open circles). The plot is complemented by four snapshots showing the control (c,d) and the tube sample (e,f) at the onset of UV exposure (c,e) and 15 h later (d,f). Notice that only frame f shows low fluorescence intensities. Although the control experiment shows a slight decay in fluorescence, it is obvious that the tube fragments accelerate the process significantly. These results suggest that the tubes are catalytically active. The observation thus presented is remarkable, as photocatalytic characteristics of metal oxide nanostructures have been rarely reported.[17]

In conclusion, we have established a reproducible and fast procedure for the self-controlling synthesis of decimeter-long silica tubes that support zinc oxide nanostructures on their interior surface. On a macroscopic scale, the tubular structures are very straight owing to the introduction of single gas bubbles. These bubbles act as buoyant templates for the growing tubes and also seem to control the tube radius. Future studies might be able to exploit the presence of these bubbles to dope the tube walls during the growth process. Moreover, a wide range of reactants and reactant mixtures are expected to yield similar structures. Accordingly, the synthesis of other support matrices, such as borates and carbonates, should be possible, and also the inclusion of other metal oxides (e.g. CuO/ZnO). Among other applications, one can envision the use of these tubes in microfluidic devices to add specific catalytic or sensor-like features.

Experimental Section

The synthesis of the tubes is performed at (25 ± 1)°C using aqueous solutions of zinc(II) sulfate ($ZnSO_4 \cdot 7H_2O$, Spectrum) and sodium silicate ($Na_2SiO_3 \cdot 5H_2O$, Fisher). All solutions are prepared with nanopure water (18 MΩ cm; EASYpure UV, Barnstead). A syringe pump (KD Scientific 200) was used to inject the zinc solution (0.5 M) through a vertical glass capillary into a large cylindrical reservoir of silicate solution (1.0 M). The flow rate was kept constant at 10.0 mL h^{-1}. The long needle of a small syringe was connected through the capillary bore, allowing the placement of single air bubbles at the nozzle. Bubble volumes range from 0.1 to 1 μL. The synthesized tubes were washed, dried overnight at room temperature, and then heated to 200–250 °C for 2 h. We estimate that the ZnO yield is approximately 60–70 %.

Characterization: SEM images were recorded on a JEOL JSM-5900 scanning electron microscope with an energy-dispersive X-ray (EDS) attachment operating at 15 kV. TEM images were acquired on a JEOL 2010 transmission electron microscope operated at 200 kV. Powder X-ray diffraction data were taken on a Siemens D500 model using the $Cu_{K\alpha}$ line ($\lambda = 1.54$ Å). Photoluminescence measurements were performed on a Spex Fluorolog τ-2 spectrofluorometer using an excitation wavelength of 325 nm (Coherent I-308 argon-ion laser).

Photocatalytic measurements: Heat-activated precipitation tubes were immersed in 100 μL of an unstirred, aqueous rhodamine B solution (5 μm) and irradiated through a quartz window with a 4 W UV lamp (Model 22-UV Lasercraft Inc.). The incident light intensity was 1.1 $mW\,cm^{-2}$. Fluorescence was measured with a Nikon digital camera at typical rates of 1 frame/hour. The decay of the fluorescence intensity is monitored by analyzing the signal of the red channel from the digital camera.

Received: July 2, 2008
Published online: November 10, 2008

Keywords: colloids · dissipative processes · photocatalysis · template synthesis · zinc oxide

[1] D. D. Double, A. Hellawell, S. J. Perry, *Proc. R. Soc. London Ser. A* **1978**, *359*, 435.
[2] J. M. García-Ruiz, S. T. Hyde, A. M. Carnerup, A. G. Christy, M. J. Van Kranendonk, N. J. Welham, *Science* **2003**, *302*, 1194.
[3] D. A. Stone, R. E. Goldstein, *Proc. Natl. Acad. Sci. USA* **2004**, *101*, 11537.
[4] M. B. Short, J. C. Baygents, J. W. Beck, D. A. Stone, R. S. Toomey, R. E. Goldstein, *Phys. Rev. Lett.* **2005**, *94*, 018501.
[5] J. B. Corliss, J. Dymond, L. I. Gordon, J. M. Edmond, R. P. Von Herzen, R. D. Ballard, K. Green, D. Williams, A. Bainbridge, K. Crane, Tj. H. van Andel, *Science* **1979**, *203*, 1073.
[6] a) J. H. E. Cartwright, J. M. García-Ruiz, M. L. Novella, F. Otálora, *J. Colloid Interface Sci.* **2002**, *256*, 351; b) J. Pantaleone, A. Toth, D. Horvath, J. R. McMahan, R. Smith, D. Butki, J. Braden, E. Mathews, H. Geri, J. Maselko, *Phys. Rev. E* **2008**, *77*, 046207.
[7] a) C. Collins, G. Mann, E. Hoppe, T. Duggal, T. L. Barr, J. Klinowski, *Phys. Chem. Chem. Phys.* **1999**, *1*, 3685; b) C. Collins, R. Mokaya, J. Klinowski, *Phys. Chem. Chem. Phys.* **1999**, *1*, 4669.
[8] S. Thouvenel-Romans, O. Steinbock, *J. Am. Chem. Soc.* **2003**, *125*, 4338.
[9] a) S. Thouvenel-Romans, W. van Saarloos, O. Steinbock, *Europhys. Lett.* **2004**, *67*, 42; b) S. Thouvenel-Romans, J. J. Pagano, O. Steinbock, *Phys. Chem. Chem. Phys.* **2005**, *7*, 2610; c) J. J. Pagano, T. Bánsági, Jr., O. Steinbock, *J. Phys. Chem. C* **2007**, *111*, 9324; d) J. J. Pagano, S. Thouvenel-Romans, O. Steinbock, *Phys. Chem. Chem. Phys.* **2007**, *9*, 110.
[10] Á. Tóth, D. Horváth, R. Smith, J. R. McMahan, J. Maselko, *J. Phys. Chem. C* **2007**, *111*, 14762.
[11] J. Maselko, P. Strizhak, *J. Phys. Chem. B* **2004**, *108*, 4937.
[12] H. R. Oswald, R. Asper in *Preparation and Crystal Growth of Materials with Layered Structures* (Ed.: R. M. A. Lieth), Kluwer, Dordrecht, **1977**, p. 128.
[13] a) M. H. Huang, Y. Y. Wu, H. Feick, N. Tran, E. Weber, P. D. Yang, *Adv. Mater.* **2001**, *13*, 113; b) S. L. Mensah, V. K. Kayastha, I. N. Ivanov, D. B. Geohegan, Y. K. Yap, *Appl. Phys. Lett.* **2007**, *90*, 113108.
[14] A. Mikrajuddin, F. Iskandar, K. Okuyama, F. G. Shi, *J. Appl. Phys.* **2001**, *89*, 6431.
[15] C. Xu, J. Chun, K. Rho, D. E. Kim, *Nanotechnology* **2005**, *16*, 2808.
[16] K. Vanheusden, W. L. Warren, C. H. Seager, D. R. Tallant, J. A. Voight, B. E. Gnade, *J. Appl. Phys.* **1996**, *79*, 7983.
[17] J. L. Yang, S. J. An, W. I. Park, G.-C. Yi, W. Choi, *Adv. Mater.* **2004**, *16*, 1661.